Korean J. Math. **33** (2025), No. 2, pp. 181–192
https://dx.doi.org/10.11568/kjm.2025.33.2.181

DYNAMIC MODE DECOMPOSITION BASED PREDICTION METHOD FOR DIFFUSIVE LOTKA-VOLTERRA EQUATION

Donghyun Kim

Abstract. In this work, we propose a dynamic mode decomposition (DMD) based prediction method for diffusive Lotka-Volterra equations. To accommodate the multi-species structure of the model, we concatenate the solutions of all species into a single snapshot. Once the DMD modes are extracted, we can separate the modes of each species easily. While each species exhibits distinct mode shapes, they share identical eigenvalues, indicating that interspecies interactions are captured. Snapshot data are first generated using a finite difference method, and long-term predictions are then obtained via the DMD reconstruction. From these predictions, we reconstruct the species dominance indicator function, which classifies the dominant species at each spatial location. Numerical experiments demonstrate that the DMD based predictions for dominance indicator function achieves high accuracy while effectively reducing computational cost.

1. Introduction

The Lotka-Volterra (LV) equation, which describes the dynamics of predator-prey interactions, plays an important role in ecology and biology [1–4]. The populations (or density) of variables of species in LV equation is under the effects of the inter-species limiting effects described by nonlinear reaction terms. Since predator-prey interaction model can be applied in various situations, there have been many researches of applying LV equation in other areas, for example competition models in economics [5] and technology adoption model in ecosystem [6]. Given their versatility, various extensions of the original LV equations have been developed to address specific scenarios. Among them, a practical modification is to include the spatial diffusion term in the LV model [7, 8], which results in a reactive LV equation [9, 10]. Using these model, one can study the spatiotemporal patterns in predator-prey model.

Due to the significance in understanding complex dynamic across the species, various numerical methods for solving diffusive LV model have been developed. For example, finite difference/element method (FDM/FEM) based approaches were developed in [11–14] while finite volume method (FVM) based version can be found in [15]. One of the difficulties in solving diffusive LV-type equations is the nonlinear term. When employing forward Euler type methods, people usually employ Runge-Kutta methods (RK) [19]. However, one needs to be careful about the stability

Received April 7, 2025. Revised May 18, 2025. Accepted June 9, 2025.
2010 Mathematics Subject Classification: 65M22, 35Q92, 65M25.
Key words and phrases: Diffusive Lotka-Volterra, Dynamic Mode Decomposition, Data Driven.

conditions. On the other hand, implicit methods like the backward Euler scheme results in relatively stable numerical solutions since in each time step equilibrium must be satisfied. However, those methods require certain linearization techniques such as the Newton-Raphson method, which often include computationally expensive matrix solving steps. Therefore, alternative approaches are required to efficiently solve the diffusive LV model.

Meanwhile, dynamic mode decomposition (DMD) has emerged as a data-driven algorithm for analyzing partial differential equations (PDEs) [16–18]. The main idea of DMD is to approximate the operator of the PDEs using the the snapshot type of dataset. By extracting certain number of modes and corresponding eigenvalues, one can determine the growing or decreasing factors inside the solution sets. One key advantage of using (small) number of modes is the natural suppression of high-frequency noises possibly obtained in measurement. By representing the snapshot solutions in the linear combinations of modes, DMD methodology can be used to provide long-term prediction of the unseen solutions. Due to its simple and robust methodology, DMD has also been applied in various areas, for example in epidemiology for predicting infectious diseases [20], in neuroscience for analyzing brain activity [21], and in ecological systems for understanding species interactions over time [16].

In this study, we propose a DMD based prediction method for diffusive LV systems. While we need to consider multi-variable solutions in diffusive LV systems, standard DMD algorithm are mostly designed for single-variable datasets. To remedy this, we slightly modified conventional DMD by concatenating the solutions of each species in a single snapshot. This modification allows us to generate DMD modes for all species simultaneously, effectively capturing the coupled dynamics of the system. We remark that while each species exhibits distinct DMD mode shapes, they share identical eigenvalues. We may conclude that interspecies interactions are effectively encapsulated within the shared eigenvalues. The predictive capability of our approach is demonstrated by reconstructing the dominance indicator function, achieving an accuracy exceeding 92 percent for predictions extending 150 seconds into the future. In terms of computational efficiency, the DMD-based predictions require only approximately 5 percent of the CPU time needed for generating solutions using FDM. This reduction in computational cost highlights the practicality of the DMD approach for efficient analysis of multi-species diffusive systems. As far as the author acknowledges, this work is the first successful application of DMD for the diffusive type LV systems.

The rest of the section is organized as follows. In Section 2, the DMD based prediction method for diffusive LK system is proposed. In Section 3, we give numerical results. Conclusion follows in Section 4

2. Method

2.1. Governing equation. In this work, we describe the spatial diffusive LV model [14]. For the convenience's sake, we consider three interacting species in a bounded

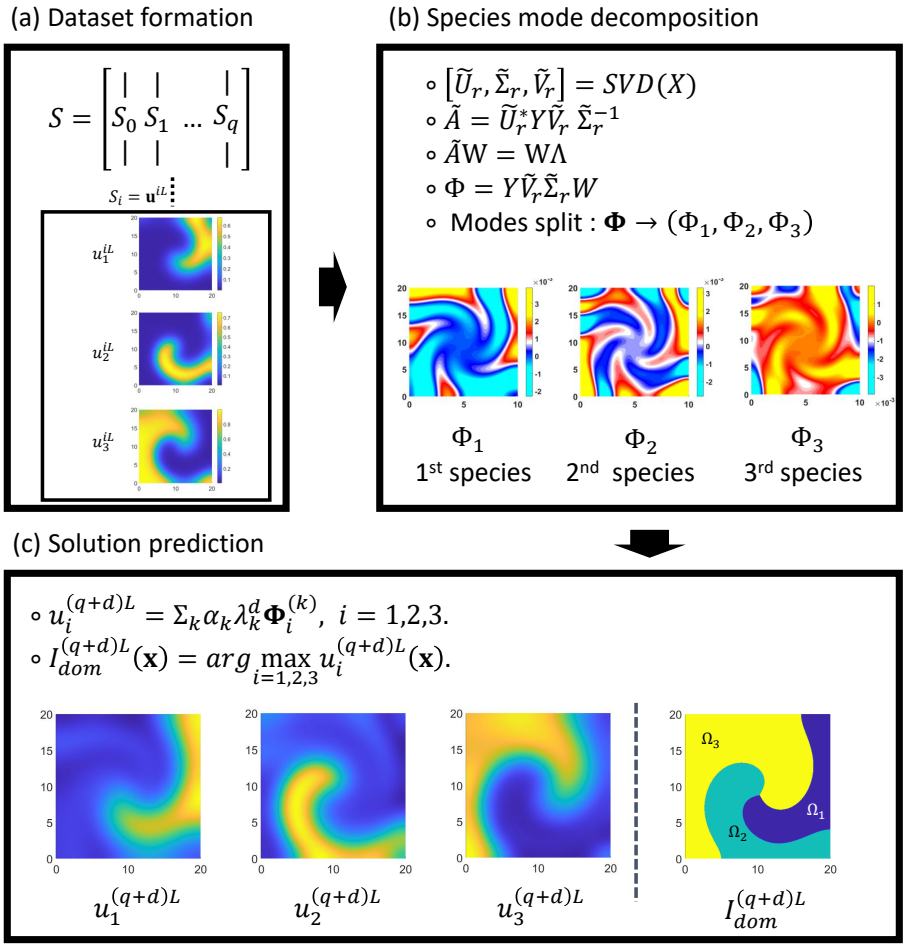

FIGURE 1. Description of overall process.

domain $\Omega = [0, M]^2 \subset \mathbb{R}^2$. The governing equation is described as follows:

$$\frac{\partial u_1}{\partial t} - \epsilon_1 \Delta u_1 = a_1 u_1 (1 - \alpha_{1,1} u_1 - \alpha_{1,2} u_2 - \alpha_{1,3} u_3) \quad \text{on } \Omega \times \mathbb{R}^+, \tag{1}$$

$$\frac{\partial u_2}{\partial t} - \epsilon_2 \Delta u_2 = a_2 u_2 (1 - \alpha_{2,1} u_1 - \alpha_{2,2} u_2 - \alpha_{2,3} u_3) \quad \text{on } \Omega \times \mathbb{R}^+, \tag{2}$$

$$\frac{\partial u_3}{\partial t} - \epsilon_3 \Delta u_3 = a_3 u_3 (1 - \alpha_{3,1} u_1 - \alpha_{3,2} u_2 - \alpha_{3,3} u_3) \quad \text{on } \Omega \times \mathbb{R}^+. \tag{3}$$

where the primary variable $u_i(\mathbf{x}, t)$ stands for the density of the species i. The parameters ϵ_i denotes the diffusion rate of each species, a_i the natural growth of species, and $\alpha_{i,j}$ the competition. Specifically, $\alpha_{i,j}$ quantify the limiting effects of species j on species i. In the presence of large values of $\alpha_{i,j}$, species j has a more significant competitive effect on species i. For the well posedness of the problem we need boundary and initial value conditions.

$$\frac{\partial u_i}{\partial \mathbf{n}} = 0, \quad \text{on } \partial\Omega \tag{4}$$

$$u_i(\mathbf{x}, 0) = g_i, \quad \text{on } \Omega. \tag{5}$$

THEOREM 2.1. *[22] The equations (1)-(5) determine the unique solution.*

2.2. FDM based methods for generating dataset. To be able to apply DMD, we need to first numerically solve the governing equations. Also, suppose ΔT is used for the timestep. We use the notation $u_i(t = n\Delta T) = u_i^n$, $i = 1, 2, 3$ and

$$\mathbf{u}^\ell = [u_1^\ell, u_2^\ell, u_3^\ell], \quad \ell = 0, 1, \dots.$$

We first describe the time discretization. Crank Nicolson type is employed to obtain the accurate solutions:

$$\frac{u_i^{n+1} - u_i^n}{\Delta T} = \frac{1}{2}\left(\epsilon_i \Delta u_i^{n+1} + \epsilon_i \Delta u_i^n\right) + [\mathcal{R}(\mathbf{u}^n, \mathbf{u}^{n-1})]_i, \quad i = 1, 2, 3, \tag{6}$$

where

$$[\mathcal{R}(\mathbf{u}^n, \mathbf{u}^{n-1})]_i = \frac{3}{2} a_i u_i^n (1 - \sum_j \alpha_{i,j} u_j^n) - \frac{1}{2} a_i u_i^{n-1} (1 - \sum_j \alpha_{i,j} u_j^{n-1}), \quad i = 1, 2, 3.$$

Then, it remains to describe the spatial discretization. We only briefly describe the FDM implementation, since it is already well known. Suppose the domain is discretized with uniform grid of size h resulting in $m \times m$ number of nodes. Then, u_i and $\mathbf{u}$ has m^2 and $3m^2$ number of degrees of freedom respectively. Suppose A denotes the $m^2 \times m^2$ matrix arising from the FDM implementation of Poisson equation, $-\Delta u = f$, in the uniform grids. Then, (6) can be compactly written as:

$$\left(I + \frac{\Delta T}{2}\mathcal{D}\right)\mathbf{u}^{n+1} = \mathbf{u}^n - \frac{\Delta T}{2}\mathcal{D}\mathbf{u}^n + \Delta T \mathcal{R}(\mathbf{u}^n, \mathbf{u}^{n-1}), \quad i = 1, 2, 3, \tag{7}$$

where

$$\mathcal{D} = \begin{bmatrix} \epsilon_1 A & 0 & 0 \\ 0 & \epsilon_2 A & 0 \\ 0 & 0 & \epsilon_3 A \end{bmatrix}.$$

We note that, to obtain $\mathbf{u}^1$ from above, we need $\mathbf{u}^{-1}$ which is unavailable. Therefore, $\mathbf{u}^1$ is obtained by first order Euler backward method:

$$(I + \Delta T \mathcal{D})\,\mathbf{u}^1 = \mathbf{u}^0 - \Delta T \mathcal{D}\mathbf{u}^0 + \Delta T \mathcal{R}(\mathbf{u}^0, \mathbf{u}^0). \tag{8}$$

Let us summarize the FDM method for obtaining solutions up to time $t = N\Delta T$.

Algorithm 1: FDM for diffusive LV equation

1. Set $\mathbf{u}^0 = \mathbf{g}$ where $\mathbf{g} = (g_1, g_2, g_3)$;
2. Solve (8) to obtain $\mathbf{u}^1$;

for $n = 1, \cdots, N-1$ **do**
  Solve (7) to obtain $\mathbf{u}^{n+1}$;
end

Before closing this section, we describe the construction of the data set. First, we need to choose snapshots from the FDM generated solutions $\mathbf{u}^n$, $(n = 0, ..., N)$ using the rule

$$S_i = \mathbf{u}^{iL}, \quad i = 0, \dots, q.$$

Obviously, q is the smallest integer such that $qL \geq N$ and each S_i has $3m^2$ number of entries. We define the data set in matrix form as $S = [S_0 \,|\, \cdots \,|\, S_q]$.

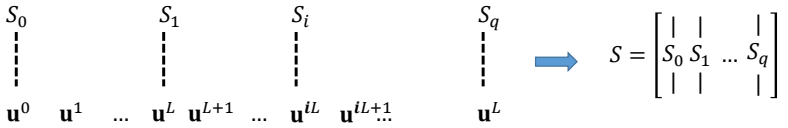

FIGURE 2. Construction of the snapshot type dataset from the FDM generated solutions.

2.3. DMD based prediction of the diffusive LV system. In this subsection, we describe DMD based prediction method for diffusive LV systems. The main idea of DMD is to analyze the mode of the operator satisfying

$$AS_i = S_{i+1}, \quad i = 0, \ldots, q-1. \tag{9}$$

Once we find A, the unseen data can be predicted easily by applying A^d to last snapshot:

$$\mathbf{u}^{(q+d)L} \approx A^d \mathbf{u}^{qL}.$$

Also, by finding the eigenvectors and eigenvalues of A, the governing equation can be analyzed. Although it is hard to find operator A which exactly satisfy (9), one can alternatively define operator as the minimizer of the least square of $||X - AY||_F$ where

$$X = \begin{bmatrix} | & \cdots & | \\ S_0 & \cdots & S_{q-1} \\ | & \cdots & | \end{bmatrix}, \qquad Y = \begin{bmatrix} | & \cdots & | \\ S_1 & \cdots & S_q \\ | & \cdots & | \end{bmatrix}.$$

We remark that the size of X is $3m^2 \times q$, when the number of nodes in meshgrid is $m \times m$. Here, $||\cdot||_F$ is the Frobenius norm. Suppose X is decomposed by truncated SVD (singular value decomposition) with rank r:

$$X \approx \tilde{U}_r \tilde{\Sigma}_r \tilde{V}_r^*,$$

where $\tilde{U}_r \in \mathbb{C}^{3m^2 \times r}$, $\tilde{\Sigma}_r \in \mathbb{C}^{r \times r}$, and $\tilde{V}_r \in \mathbb{C}^{q-1 \times r}$. The operator A can be expressed using the pseudo inverse of X,

$$A \approx YX^\dagger = Y\tilde{V}_r^* \tilde{\Sigma}_r^{-1} \tilde{U}_r^*,$$

However, computation above for obtaining A is demanding, since it includes the matrix multiplications of dense matrices of large size. In DMD methodology, modes of A is obtained alternatively using the reduced matrix $\tilde{A} := \tilde{U}_r^* A \tilde{U}_r$, which is the projected operator on the column space of $\tilde{U}_r$.

LEMMA 2.2 ([16]). *The projected operator $\tilde{A}$ is computed by*

$$\tilde{A} = \tilde{U}_r^* Y \tilde{V}_r \tilde{\Sigma}_r^{-1}.$$

Next, we diagonalize $\tilde{A}$, i.e.,

$$\tilde{A}W = W\Lambda$$

where columns of W are eigenvectors of $\tilde{A}$ and Λ is diagonal matrix. Finally, we relate the eigenvectors of $\tilde{A}$ and A.

LEMMA 2.3 ([16]). *The eigenvectors of A are given by*

$$\mathbf{\Phi} = Y\tilde{V}_r\tilde{\Sigma}_r^{-1}W$$

and the below relation holds:

$$A\mathbf{\Phi} = \mathbf{\Phi}\Lambda.$$

The columns i-th of $\mathbf{\Phi}$ are the i-th DMD modes, which we denote $\Phi^{(i)}$. Also, denote λ_i the i-th diagonal entry of Λ. Let us summarize the process of finding DMD modes.

Algorithm 2: DMD modes and eigenvalues of A

1. Compute $\tilde{A} = \tilde{U}_r^* Y\tilde{V}_r\tilde{\Sigma}_r^{-1}$;
2. Diagonalize $\tilde{A}$, i.e., $\tilde{A}W = W\Lambda$;
3. Compute DMD modes as $\Phi = Y\tilde{V}_r\tilde{\Sigma}_r^{-1}W$;

In our version, the typical snapshot S^n contains the population of three species, that is, $S^n = (u_1^{nL}, u_2^{nL}, u_3^{nL})$. Once modes $\mathbf{\Phi}^{(j)}$, $(j = 1, ..., r)$ are computed by **Algorithm 2**, we decompose them as

$$\mathbf{\Phi}^{(j)} = [\Phi_1^{(j)} \mid \Phi_2^{(j)} \mid \Phi_3^{(j)}],$$

so that each $\Phi_i^{(j)}$ has m^2 entries. Then, Φ_i represents the spatiotemporal patterns of the population of i'th species. In this way, spatiotemporal patterns of each species are extracted simultaneously. Let us remark that λ_j is a shared eigenvalue associated with $\Phi_1^{(j)}$, $\Phi_2^{(j)}$, and $\Phi_3^{(j)}$. Since same eigenvalue is shared among three species, DMD analysis for the diffusive LV equation efficiently captures the interdependent dynamics between them.

Now, let us turn to the DMD based prediction of the diffusive LV equation for the unseen data. Since our version of DMD is devoted for multivariable-type dataset, there should be some modifications in the prediction also. First, we will project S^q, which is the last snapshot data observed, to the DMD mode space. Formally, it suffices to find coefficients of the linear combination of DMD modes to reconstruct S_q : find $\beta = (\beta_1, ..., \beta_r)$ such that minimize

$$||S_q - \sum_{k=1}^{r} \beta_k \mathbf{\Phi}^{(k)}||_F. \tag{10}$$

Once the coefficients β are determined, then S_q is alternatively written as

$$S_q \approx \sum_{k=1}^{r} \beta_k \mathbf{\Phi}^{(k)}. \tag{11}$$

By multiplying A^d to the both sides, we obtain the prediction of the d times ahead unseen data :

$$S_{q+d} \approx \sum_{k=1}^{r} A^d \beta_k \mathbf{\Phi}^{(k)} = \sum_{k=1}^{r} \beta_k \lambda_k^d \mathbf{\Phi}^{(k)}.$$

Using the definitions of S_q and Φ_i, the approximated population of each species can be written as

$$u_i^{(q+d)L} \approx \sum_{k=1}^{r} \beta_k \lambda_k^d \Phi_i^{(k)}, \quad i = 1, 2, 3. \tag{12}$$

Let us briefly discuss the error estimates for the DMD prediction. In [23], error bounds for DMD predicted solutions for parabolic PDE were analyzed. The study shows that increasing the number of snapshots reduces the prediction error. On the other hand long-time predictions tend to exhibit growing errors as target prediction time increases. Although our model is multivariable case, we expect similar error behavior. In generating FDM solutions, the number of snapshots is influenced by the time step size ΔT. Therefore, choosing a reasonably small ΔT is useful for achieving robust DMD prediction.

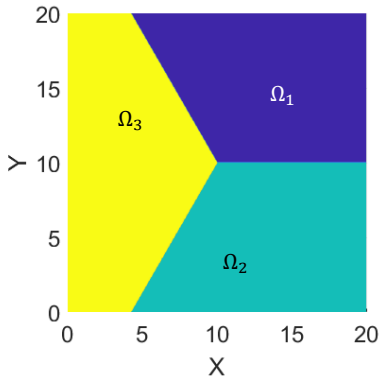

FIGURE 3. Illustration of the initial condition. The domain is partitioned into disjoint sub-regions Ω_1, Ω_2, and Ω_3. Ω_i is occupied by i-th species.

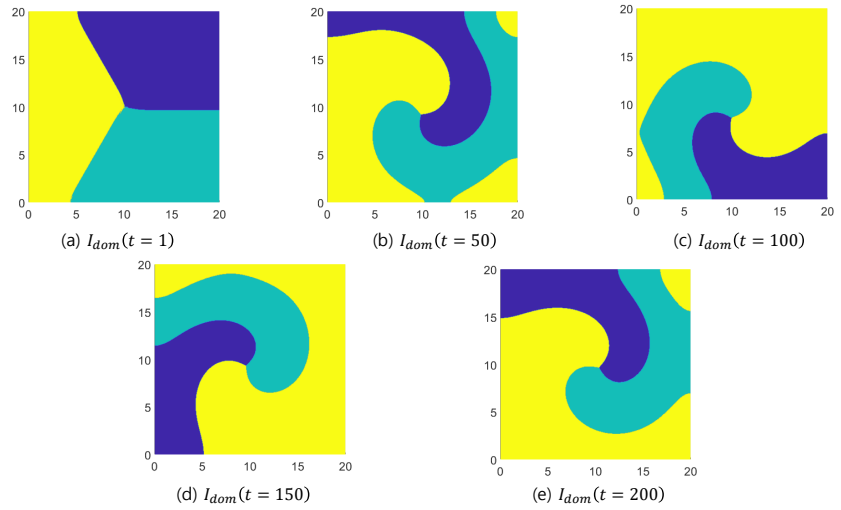

FIGURE 4. Illustration of initial condition. The domain is partitioned into disjoint sub-regions Ω_1, Ω_2, and Ω_3. Ω_i is occupied by i-th species.

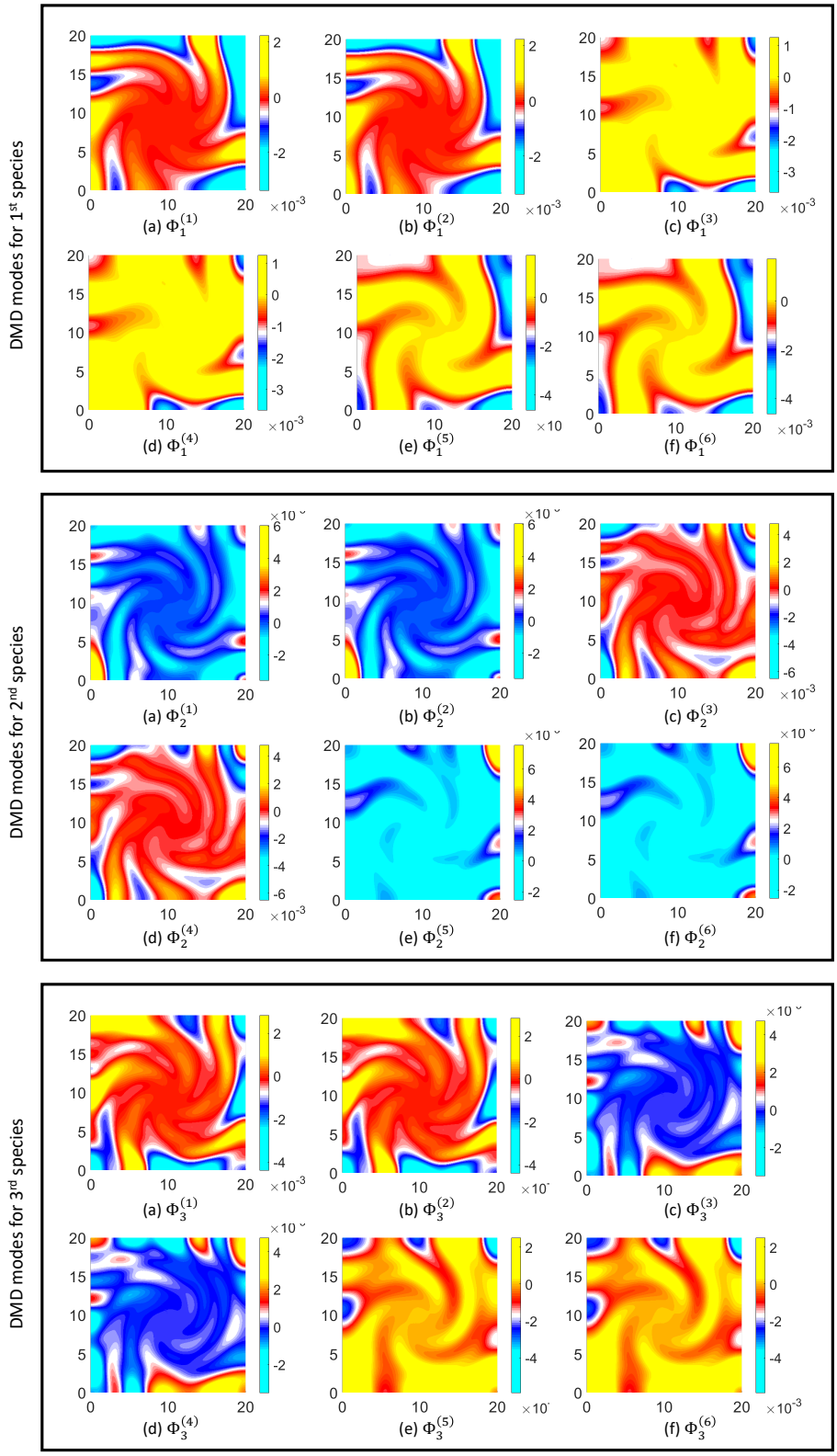

FIGURE 5. Illustration of DMD modes for u_1, u_2 and u_3.

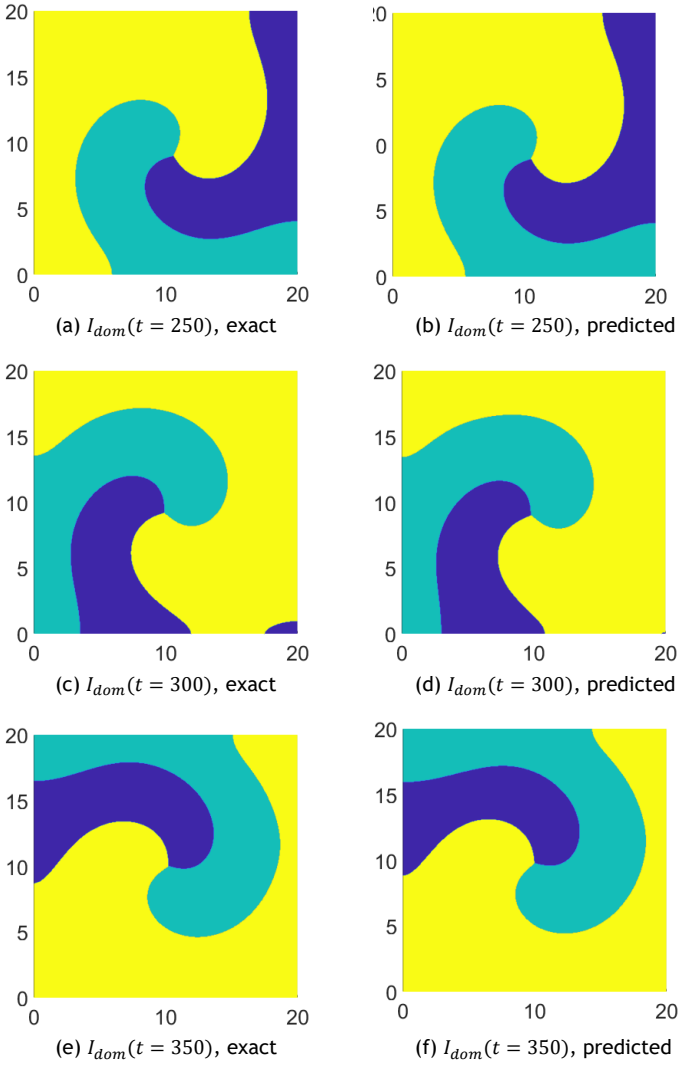

FIGURE 6. Comparison between the exact dominance indicator function and predicted indicator function.

3. Results

We now present some numerical example on domain $\Omega = [0, 20]^2$. The intrinsic growth rates are set to $a_i = 1$ for $i = 1, 2, 3$. The diffusion parameters are $\epsilon_1 = 0.7$, $\epsilon_2 = 0.2$, and $\epsilon_3 = 0.6$, respectively, reflecting heterogeneous mobility across the species. To induce cyclic dominance behavior in population dynamics, we set the competition coefficients as:

$$\alpha = \begin{bmatrix} 1 & 1 & 3 \\ 3 & 1 & 1 \\ 1 & 3 & 1 \end{bmatrix}. \tag{13}$$

This configuration promotes a rock–paper–scissors type of cycle interaction pattern, where each species dominates and is dominated by one of the others. To describe the the initial condition, we partition the domain into three disjoint subregions, i.e., $\Omega = \Omega_1 \cup \Omega_2 \cup \Omega_3$, as illustrated in Figure 3. The initial boundary conditions are given

by

$$u_i(\mathbf{x}, t = 0) = \chi_{\Omega_i}(\mathbf{x}), \quad i = 1, 2, 3,$$

where χ_A is the usual characteristic function on A. As time evolves, the density of each species is under effects of diffusion and nonlinear-inter terms. The dynamics of three species are captured efficiently by dominance indicator function

$$I_{dom}(\mathbf{x}, t) = arg \max_{i=1,2,3} u_i(\mathbf{x}, t).$$

The function $I_{dom}(\mathbf{x})$ shows which species dominate on each location$\mathbf{x}$. Since we have imposed different diffusion rates ϵ_i, the solution I_{dom} exhibits asymmetric patterns. The experiments were conducted on Intel(R) Core (TM) i9-10900X CPU.

Now, let us describe the generation of the solutions by FEM methods. The uniform grid with 401×401 number of nodes is used to discretize the spatial domain, resulting in meshsize $h = 0.05$. Since we are using Crank Nicolson type algorithm, we can assign $\Delta T = \mathcal{O}(h)$. In our version, we choose $\Delta T = h = 0.05$. Following **Algorithm** 1. The FDM generated solutions at $t = 1$, 50, 100, 150, 200 are depicted in Figure 4. Clearly, we observe cyclic behavior of the regions dominated by each species.

Next, to generate the dataset S, a sampling interval of $L = 20$ is chosen, corresponding to a temporal gap of 1 second between between S_i and S_{i+1}. Empirically, at least 100 snapshots are required to achieve reasonably small reconstruction errors. With the choice of sampling interval $L = 20$, we were able to obtain 200 number of snapshots.

Using **Algorithm** 2, we generate $r = 41$ number of DMD modes. The choice of parameter $r = 41$ will be justified at the end of this section. Figure 5 shows the first six modes of each species. We can observe that cyclic patterns appear in the DMD modes, which is inherent to the predefined competing coefficient α.

Finally, let us present the long time-prediction of the unseen data. We first represent solution $u_i(t = 200)$ by the linear combinations of DMD modes as in (11). Then, prediction of $\tilde{u}_i$ is obtained using (12). The dominance indicator is then reconstructed as $I_{dom}(\mathbf{x}, t) = arg \max_{i=1,2,3} \tilde{u}_i(\mathbf{x}, t)$. Figure 6 compares the true dominance indicators with the reconstructed dominance indicator at $t = 250$, 300, and 350. We observe that overall the reconstructed solution matches the true solution. The accuracy was 97.28%, 94.47%, and 94.59% at $t = 250$, 300, and 350. Notably, the DMD-based predictions are computationally efficient, requiring only 4.9 seconds to generate solution at $t = 350$. In contrast, computing the FDM solutions from $t = 200$ to $t = 350$ takes 1,943 seconds. Thus, the DMD approach uses only approximately 0.25% of the CPU time required by the FDM method.

Before closing this section, let us provide the justification for choosing the number of DMD modes. Table 1 shows the prediction accuracy for $I_{dom}(\mathbf{x}, t)$ with various choice of r. If too small number of DMD modes are used ($r = 5, 11$), we have low accuracy ($< 90\%$). However, increasing r does not always lead to better accuracy. Therefore, we may conclude that choosing excessively large value for r does not capture the spatiotemporal patterns. Based on Table 1, we choose the parameter $r = 41$, which yields the highest accuracy when $t = 350$ seconds.

TABLE 1. Prediction accuracy of I_{dom} by DMD for various values of r.

r	$I_{dom}(t=250)$	$I_{dom}(t=300)$	$I_{dom}(t=350)$
5	50.85%	12.58 %	3.89 %
11	89.45%	87.77 %	81.56 %
21	94.03%	94.02 %	91.64 %
41	97.28%	94.47 %	94.59 %
61	97.43%	96.60 %	92.80 %
101	97.29%	96.55 %	92.92 %

4. Conclusion

In this work, we propose DMD based mode prediction method for diffusive LV equation. Since we need to consider multi variable solutions in diffusive LV systems, we define the snapshot data by concatenating the solutions of each species. One of the advantages of our frameworks is that different species shares the identical eigenvalues, indicating that ineterspecies interactions are effectively captured. In the numerical section, we provide some example. While achieving reasonable accuracy, the computational costs in DMD process was significantly reduced. The time costs used in DMD prediction was less than 5%

Competing Interests

The author declares that there is no competing interest.

References

[1] P. J. Wangersky, *Lotka-Volterra population models*, Annu. Rev. Ecol. Syst., **9** (1978), 189–218. https://www.jstor.org/stable/2096748

[2] B. Guy, *Ecological communities with Lotka-Volterra dynamics*, Phys. Rev. E, **95** (4) (2017), 042414. https://doi.org/10.1103/PhysRevE.95.042414

[3] J. He, Z. Zheng, and Z. Ye, *A new numerical approach method to solve the Lotka–Volterra predator–prey models with discrete delays*, Physica A: Stat. Mech. Appl., **635** (1) (2024), 129524. https://doi.org/10.1016/j.physa.2024.129524

[4] S. Suweis, F. Ferraro, C. Grilletta, S. Azaele, and A. Martian, *Generalized lotka-volterra systems with time correlated stochastic interactions*, Phys. Rev. Lett., **133** (16) (2024), 167101. https://doi.org/10.1103/PhysRevLett.133.167101

[5] A. W. Wijeratne, F. Yi, and J. Wei, *Bifurcation analysis in the diffusive Lotka–Volterra system: An application to market economy*, Chaos Solitons Fractals, **40** (2) (2009), 902–911. https://doi.org/10.1016/j.chaos.2007.08.043

[6] G. Zhang, D. A. McAdams, V. Shankar, and M. M. Darani, *Technology Evolution Prediction Using Lotka–Volterra Equations*, J. Mech. Des., **140** (6) (2009), 061101. https://doi.org/10.1115/1.4039448

[7] X. He and W. M. Ni, *Global dynamics of the Lotka-Volterra competition-diffusion system: Diffusion and spatial heterogeneity I.*, Commun. Pure Appl. Math., **69** (5) (2015), 981–1014. https://doi.org/10.1002/cpa.21596

[8] X. He and W. M. Ni, *The effects of diffusion and spatial variation in Lotka–Volterra competition–diffusion system I: Heterogeneity vs. homogeneity*, J. Differ. Equ., **254** (2) (2013), 528-546. https://doi.org/10.1016/j.jde.2012.08.032

[9] M. Chen, *Pattern dynamics of a Lotka-Volterra model with taxis mechanism*, Appl. Math. Comput., **471** (1) (2025), 129017.
https://doi.org/10.1016/j.amc.2024.129017
[10] Z.-A. Wang and J. Xu, *On the Lotka–Volterra competition system with dynamical resources and density-dependent diffusion*, J. Math. Biol., **82** (7) (2021), 1–37.
https://doi.org/10.1007/s00285-021-01562-w
[11] C. V. Pao and Y.-M. Wang, *Numerical solutions of a three-competition Lotka–Volterra system*, Appl. Math. Comput., **204** (1) (2008), 423–440.
https://doi.org/10.1016/j.amc.2008.06.057
[12] R. E. Mickens, *A nonstandard finite-difference scheme for the Lotka–Volterra system*, Appl. Numer. Math., **45** (2-3) (2003), 309–314.
https://doi.org/10.1016/S0168-9274(02)00223-4
[13] F. Vadillo, *Comparing stochastic Lotka–Volterra predator-prey models*, Appl. Math. Comput., **360** (1) (2019), 181–189.
https://doi.org/10.1016/j.amc.2019.05.002
[14] A. Cangiani, E. H. Georgoulis, A. Yu. Morozov, and O. J. Sutton, *Revealing new dynamical patterns in a reaction–diffusion model with cyclic competition via a novel computational framework*, Proc. R. Soc. A: Math. Phys. Eng. Sci., **474** (2018), 20170608.
https://doi.org/10.1098/rspa.2017.0608
[15] B. Andreianov, M. Bendahmane, and R. Ruiz-Baier, *Analysis of a finite volume method for a cross-diffusion model in population dynamics*, Math. Models Methods Appl. Sci., **21** (2) (2011), 307–344.
https://doi.org/10.1142/S0218202511005064
[16] P. J. Schmid, *Dynamic Mode Decomposition and Its Variants*, Annu. Rev. Fluid Mech., **54** (1) (2022), 225–254.
https://doi.org/10.1146/annurev-fluid-030121-015835
[17] J. L. Proctor, S. L. Brunton, and J. N. Kutz, *Dynamic mode decomposition with control*, SIAM J. Appl. Dyn. Syst., **15** (1) (2015), 142–161.
https://doi.org/10.1137/15M1013857
[18] P. J. Schmid, L. Li, M. P. Juniper, and O. Pust z, *Applications of the dynamic mode decomposition*, Theor. Comput. Fluid Dyn., **25** (1) (2011), 249–259.
https://doi.org/10.1007/s00162-010-0203-9
[19] J. C. Butcher, *A history of Runge-Kutta methods*, Appl. Numer. Math., **20** (3) (1996), 247–260.
https://doi.org/10.1016/0168-9274(95)00108-5
[20] J. L. Proctor and P. A. Eckhoff, *Discovering dynamic patterns from infectious disease data using dynamic mode decomposition*, Int. Health, **7** (2) (2015), 139–145.
https://doi.org/10.1093/inthealth/ihv009
[21] Y. Shiraishi, Y. Kwahara, O. Yamashita, R. Fukuma, S. Yamamoto, Y. Saitoh, H. Kishima, and T. Yanagisawa, *Neural decoding of electrocorticographic signals using dynamic mode decomposition*, J. Neural Eng., **17** (3) (2020), 036009.
https://doi.org/10.1088/1741-2552/ab8910
[22] R. S. Cantrell and C. Cosner, *Spatial Ecology via Reaction-Diffusion Equations*, John Wiley & Sons, 2004.
https://doi.org/10.1002/0470871296
[23] H. Lu and D. M. Tartakovsky, *Prediction accuracy of dynamic mode decomposition*, SIAM J. Sci. Comput., **42** (3) (2020), A1639-A1662.
https://doi.org/10.1137/19M1259948

D. Kim
Center for Regional S & T Innovation Policy, KISTEP, 27740, Korea
E-mail: guru25@kistep.re.kr